Structural and functional studies of pyruvate carboxylase regulation by cyclic di-AMP in lactic acid bacteria

Philip H. Choi[a], Thu Minh Ngoc Vu[b], Huong Thi Pham[b], Joshua J. Woodward[c], Mark S. Turner[b,d], and Liang Tong[a,1]

[a]Department of Biological Sciences, Columbia University, New York, NY 10027; [b]School of Agriculture and Food Sciences, University of Queensland, Brisbane, QLD 4072, Australia; [c]Department of Microbiology, University of Washington, Seattle, WA 98195; and [d]Queensland Alliance for Agriculture and Food Innovation, University of Queensland, Brisbane, QLD 4072, Australia

Edited by Ronald R. Breaker, Yale University, New Haven, CT, and approved July 18, 2017 (received for review March 22, 2017)

Cyclic di-3′,5′-adenosine monophosphate (c-di-AMP) is a broadly conserved bacterial second messenger that has been implicated in a wide range of cellular processes. Our earlier studies showed that c-di-AMP regulates central metabolism in *Listeria monocytogenes* by inhibiting its pyruvate carboxylase (LmPC), a biotin-dependent enzyme with biotin carboxylase (BC) and carboxyltransferase (CT) activities. We report here structural, biochemical, and functional studies on the inhibition of *Lactococcus lactis* PC (LlPC) by c-di-AMP. The compound is bound at the dimer interface of the CT domain, at a site equivalent to that in LmPC, although it has a distinct binding mode in the LlPC complex. This binding site is not well conserved among PCs, and only a subset of these bacterial enzymes are sensitive to c-di-AMP. Conformational changes in the CT dimer induced by c-di-AMP binding may be the molecular mechanism for its inhibitory activity. Mutations of residues in the binding site can abolish c-di-AMP inhibition. In *L. lactis*, LlPC is required for efficient milk acidification through its essential role in aspartate biosynthesis. The aspartate pool in *L. lactis* is negatively regulated by c-di-AMP, and high aspartate levels can be restored by expression of a c-di-AMP–insensitive LlPC. LlPC has high intrinsic catalytic activity and is not sensitive to acetyl-CoA activation, in contrast to other PC enzymes.

aspartate biosynthesis | pyruvate carboxylase | cyclic di-AMP

Bacteria use various signaling molecules to regulate their complex physiology. Cyclic di-3′,5′-adenosine monophosphate (c-di-AMP) has emerged as a broadly conserved bacterial second messenger that has been implicated in a wide range of cellular processes, including cell wall homeostasis (1–3), biofilm formation (4, 5), central metabolism (6), osmoregulation (7, 8), and potassium transport (9). In various pathogenic bacteria, c-di-AMP is essential for mediating host–pathogen interactions and promoting virulence (1, 10–13). The machineries for the synthesis of c-di-AMP by diadenylate cyclases and for the degradation by phosphodiesterases are generally well conserved among bacteria (14, 15).

A wealth of crystal structures of protein targets in complex with c-di-AMP has been reported recently, providing insight into the molecular mechanisms of c-di-AMP regulation of cellular targets. These proteins generally mediate known functions of c-di-AMP in bacteria, including metabolism (6), potassium conductance (16, 17), and osmoregulation (7, 8), while some of them have unknown functions (18–21). Overall, these structures reveal that there is not a single, well-conserved binding motif, but rather many different ways of recognizing c-di-AMP. Moreover, the compound itself can adopt diverse conformations to fit into the unique binding pocket present in each target. In some structures, c-di-AMP binds symmetrically to a dimeric protein (6, 7, 16, 17), while in others c-di-AMP binds in an asymmetric fashion, with each adenine being recognized differently (5, 15, 18, 20, 21). In many structures, c-di-AMP adopts a U-shaped structure, with the two adenine bases forming the walls of the U, while in others, it is found in a more extended configuration.

We established earlier that c-di-AMP is an allosteric inhibitor of the central metabolic enzyme pyruvate carboxylase in the human pathogen *Listeria monocytogenes* (LmPC) (6). Pyruvate carboxylase (PC) is a biotin-dependent, single-chain, multidomain enzyme that forms a 500-kDa tetramer and is conserved among most organisms, from bacteria to humans (22, 23), while in a collection of Gram-negative bacteria PC contains two subunits with the stoichiometry $\alpha_2\beta_4$ (24). PC catalyzes the ATP-dependent carboxylation of pyruvate to produce oxaloacetate. The biotin, covalently linked to the biotin carboxyl carrier protein (BCCP) domain, is carboxylated in an ATP-dependent reaction in the biotin carboxylase (BC) domain (Fig. 1*A*). Subsequently, the carboxyl group is transferred from carboxybiotin to the pyruvate substrate in the carboxyltransferase (CT) domain. Due to a truncated TCA cycle in *L. monocytogenes* (25), excessive LmPC activity due to low c-di-AMP levels causes an overproduction of the downstream metabolites glutamate and citrate, resulting in a metabolic imbalance. This metabolic regulation of LmPC mediated by c-di-AMP levels is crucial for the virulence of the bacterium (6, 26).

The crystal structure of LmPC in complex with c-di-AMP gives molecular insights into its mechanism of regulation (6). The c-di-AMP binding site is at a previously unrecognized region at the CT dimer interface, far from the BC and CT active sites, indicating that the inhibition is allosteric. Surprisingly, the c-di-AMP binding pocket in LmPC is poorly conserved among bacteria, even among those that use c-di-AMP, suggesting that PC is a molecular target of c-di-AMP in only a subset of the bacteria. Based on the sequence analysis of bacterial PCs, we identified and confirmed that the PC from the human pathogen *Enterococcus faecalis* (EfPC)

Significance

Cyclic di-3′,5′-adenosine monophosphate (c-di-AMP) is a broadly conserved bacterial second messenger that has been implicated in a wide range of cellular processes. We report here structural, biochemical, and functional studies on the inhibition of *Lactococcus lactis* pyruvate carboxylase (LlPC) by c-di-AMP. The compound has a distinct binding mode in LlPC compared with that in *Listeria monocytogenes* PC. Mutations of residues in the binding site can abolish c-di-AMP inhibition. LlPC is required for efficient milk acidification through its essential role in aspartate biosynthesis. The aspartate pool in *L. lactis* is negatively regulated by c-di-AMP, and high aspartate levels can be restored by a c-di-AMP–insensitive LlPC. LlPC has high intrinsic catalytic activity and is insensitive to acetyl-CoA activation, in contrast to other PCs.

Author contributions: P.H.C., T.M.N.V., H.T.P., M.S.T., and L.T. designed research; P.H.C., T.M.N.V., H.T.P., M.S.T., and L.T. performed research; J.J.W. contributed new reagents/analytic tools; P.H.C., T.M.N.V., H.T.P., M.S.T., and L.T. analyzed data; and P.H.C., T.M.N.V., H.T.P., M.S.T., and L.T. wrote the paper.

The authors declare no conflict of interest.

This article is a PNAS Direct Submission.

Data deposition: The atomic coordinates and structure factors have been deposited in the Protein Data Bank, www.wwpdb.org (PDB ID codes 5VYW, 5VYZ, and 5VZ0).

[1]To whom correspondence should be addressed. Email: ltong@columbia.edu.

This article contains supporting information online at www.pnas.org/lookup/suppl/doi:10.1073/pnas.1704756114/-/DCSupplemental.

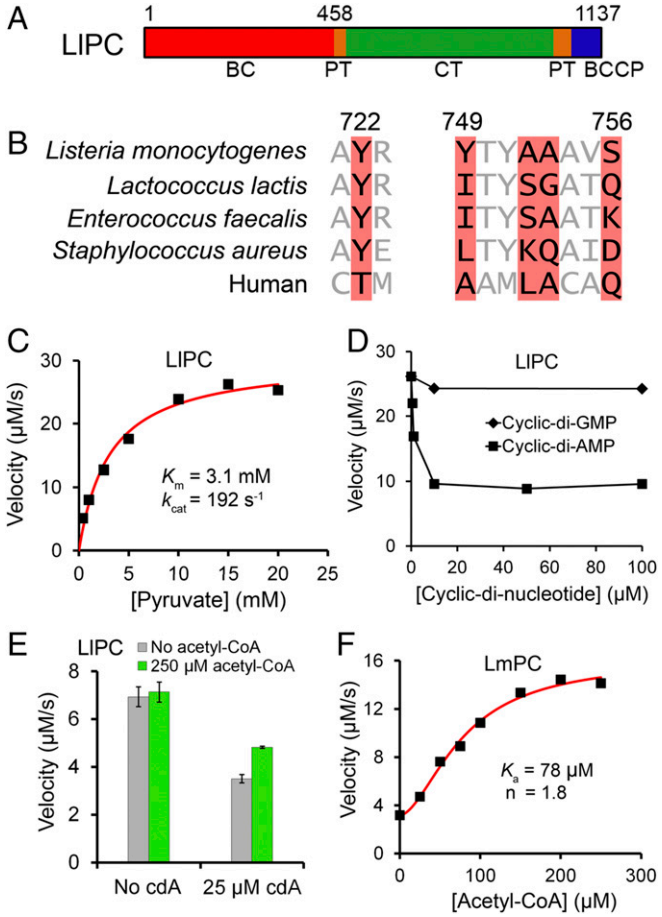

Fig. 1. Biochemical characterization of LlPC regulation by c-di-AMP. (*A*) Domain organization of LlPC. The BC, CT, BCCP, and PT domains are indicated. (*B*) Conservation of residues in the c-di-AMP binding site of LmPC (highlighted in red). The equivalent residues in selected bacterial PCs and human PC are shown. The residue numbers are for LmPC. (*C*) The catalytic activity of LlPC toward the pyruvate substrate obeys Michaelis–Menten kinetics. The reaction contained 0.16 μM LlPC (measured based on monomer). (*D*) Inhibition of the catalytic activity of LlPC by increasing concentrations of c-di-AMP and c-di-GMP. The reaction contained 0.16 μM LlPC and 20 mM pyruvate. (*E*) Acetyl-CoA has essentially no effect on the catalytic activity of free LlPC, and only a small effect in the presence of c-di-AMP. The reaction contained 0.12 μM LlPC and 3 mM pyruvate. Error bars represent SDs over three separate experiments. (*F*) Acetyl-CoA leads to a significant activation of LmPC. The reaction contained 0.78 μM LmPC and 0.5 mM pyruvate.

also binds and is regulated by c-di-AMP (6). However, there are differences in the residues composing the EfPC binding pocket compared with those in LmPC (Fig. 1*B*), suggesting that the c-di-AMP binding mode in EfPC may be different.

In this study, we have extended the c-di-AMP regulation of PC to *Lactococcus lactis*, a closely related bacterium to *E. faecalis*. We have determined the crystal structure of *L. lactis* PC (LlPC) in complex with c-di-AMP at 2.3-Å resolution. Biochemical studies on LlPC show that, in addition to being inhibited by c-di-AMP, it has several unique features including intrinsically high enzymatic activity while being insensitive to acetyl-CoA activation. We have also carried out functional studies to assess the importance of LlPC regulation by c-di-AMP, and its essential role in the biosynthesis of the amino acid aspartate.

Results

Identification of LlPC as a c-di-AMP Target. The structure of LmPC revealed residues that are important for c-di-AMP binding (Fig. 1*B*) (6). We searched through available bacterial PC sequences to identify additional PCs that could also be regulated by c-di-AMP. Based on these sequence comparisons, we identified the PC from the opportunistic pathogen *Enterococcus faecalis* (EfPC) and the industrially important *Lactococcus lactis* (LlPC) as good candidates for c-di-AMP binding (Fig. 1*B*), with both species being members of the large clade of lactic-acid bacteria. EfPC (6) and LlPC (27) have high sequence conservation both overall (72% identity) and in the putative c-di-AMP binding pocket (Fig. 1*B*). They share the Tyr722 residue (LmPC numbering) that is critical for interacting with the adenine base of c-di-AMP, and have small residues at positions 752–753, which is necessary for providing space for c-di-AMP binding. However, the other residues in the c-di-AMP binding pocket have substantial differences with LmPC (Fig. 1*B*). While these differences probably will not preclude the binding of c-di-AMP altogether, they may affect the binding mode of the compound.

We expressed and purified LlPC in a fully biotinylated and catalytically active form (Fig. 1*C*) and found that c-di-AMP at 10 μM concentration inhibited LlPC activity by ∼60% (Fig. 1*D*), to a similar degree as LmPC (6). The inhibition remained at ∼60% even with 100 μM c-di-AMP, which was also observed for LmPC (6), and the mechanism for this is not clear. No inhibition is observed with c-di-GMP, confirming the specificity of the regulation (Fig. 1*D*).

Acetyl-CoA is a well-characterized allosteric activator of single-chain PC enzymes (22, 23). LlPC has a conserved acetyl-CoA binding site, but to our surprise it was essentially insensitive to acetyl-CoA activation even with high concentrations of the compound (Fig. 1*E*). In comparison, acetyl-CoA increased LmPC activity by about fourfold, with an activation constant (K_a) of 78 μM and a Hill coefficient of 1.8 (Fig. 1*F*). Earlier studies on *Staphylococcus aureus* PC (SaPC) showed hyperbolic activation by acetyl-CoA, with K_a of 2 μM (28). In the presence of saturating c-di-AMP inhibition, LlPC is activated ∼30% by acetyl-CoA (Fig. 1*E*), but this level of activation is well below that observed in other PC enzymes (29). To our knowledge, LlPC is the only single-chain PC studied to date that is not substantially activated by acetyl-CoA (29).

LlPC has a k_{cat} of 192 s^{-1} (Fig. 1*C*), which is significantly higher than most PC enzymes studied to date. For example, SaPC has a k_{cat} of 20 s^{-1} in the absence of acetyl-CoA (30). However, the k_{cat} increases by approximately sixfold in the presence of acetyl-CoA, which would make it comparable to that for LlPC. Therefore, LlPC appears to be in a constitutively activated state, which may explain why it is not sensitive to acetyl-CoA.

Crystal Structure of LlPC in Complex with c-di-AMP. Next, we determined the crystal structure of LlPC in complex with c-di-AMP at 2.3-Å resolution (Table S1). A tetramer of LlPC was observed in the crystal (Fig. 2*A*), consistent with previously reported structures of *Rhizobium etli* PC (RePC) (31), SaPC (28), and LmPC (6), and the migration behavior of LlPC on a gel filtration column is similar to that of SaPC and LmPC. Mg-ADP is bound in each of the four BC active sites, and three of the B subdomains of BC are ordered and in a closed conformation. ATP was added before crystallization and may have hydrolyzed to ADP. While a citrate molecule from the crystallization solution was present in the acetyl-CoA binding pocket in the LmPC structure, the acetyl-CoA binding pocket is not occupied in the LlPC structure.

The LlPC tetramer is similar in overall structure to previously determined PC structures, with two monomers each in the top and bottom layers of the tetramer (Fig. 2*A*). Contacts between monomers are mediated primarily by the BC and CT dimers, which are located at opposite corners of the square-shaped tetramer. As in the LmPC structure (6), the PC tetramerization (PT) domains do not interact with each other in the tetramer in the c-di-AMP complex. LlPC shares 63% sequence identity with LmPC, and the overall structures of the two tetramers are similar as well (Fig. S1).

All four BCCP domains are well ordered in the LlPC structure and have nearly identical conformations in the tetramer. In

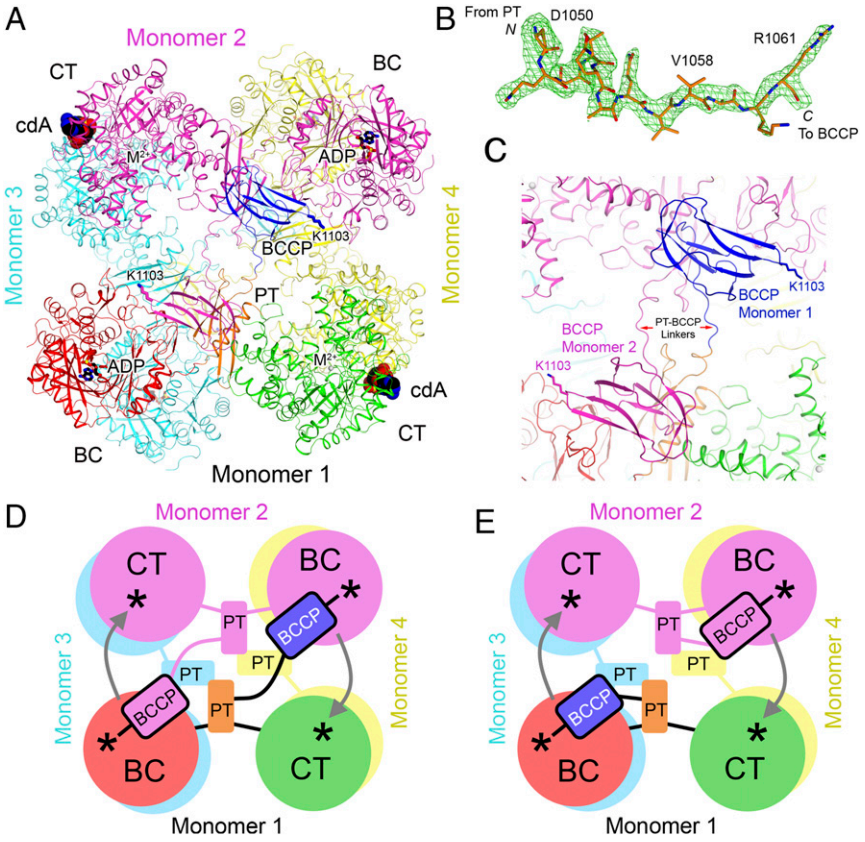

Fig. 2. Crystal structure of LlPC in complex with c-di-AMP. (*A*) Schematic drawing of the structure of LlPC tetramer in complex with c-di-AMP. Monomer 1 is colored as in Fig. 1*A*; monomer 2, in magenta; monomer 3, in cyan; and monomer 4, in yellow. c-di-AMP is shown as a sphere drawing (in black for carbon atoms, labeled cdA). (*B*) Omit F_o–F_c electron density at 2.3-Å resolution for the PT–BCCP linker in LlPC, contoured at 3σ. (*C*) Close-up showing the connection between PT and BCCP domains in the LlPC tetramer in complex with c-di-AMP. (*D*) Schematic drawing for an alternative model for PC catalysis where BCCP visits the BC active site of the other monomer in the same layer of the tetramer, and then visits the CT active site of its own monomer for catalysis. The BC and CT active sites are indicated with the asterisks, and the arrows indicate BCCP translocation during catalysis. (*E*) A previously proposed model for PC catalysis (28, 31), where BCCP visits the BC active site of its own monomer and then the CT active site of the other monomer.

contrast to the LmPC structure, electron density for the PT–BCCP linker in LlPC is clearly visible in all four monomers (Fig. 2*B*), allowing for unambiguous assignment of the BCCP domains to each monomer. The BCCP domains are swapped between monomers in the same layer of the tetramer, with each BCCP making extensive contacts with the PT domain of the opposite monomer, burying 800 Å^2 of surface area (Fig. 2*C*). This BCCP–PT interface is predominantly composed of hydrophilic residues, and has previously not been observed in PC crystal structures, although the BCCP has been found in a similar location in cryo-EM reconstructions of SaPC (32, 33). The BCCP domain comes into close proximity with the BC domain of the opposite monomer, and Lys1103 to which the biotin is covalently attached is located only 20 Å from the BC active site. The biotin moiety itself is projected into solution and is disordered in the current structure. The location of BCCP in close proximity to the BC domain of the opposite monomer in LlPC suggests an alternative mechanism for PC catalysis (Fig. 2*D*), in contrast to earlier observations on RePC and SaPC that suggest BCCP visits the BC active site of its own monomer during catalysis (Fig. 2*E*) (28, 31). It is also possible that this alternative mechanism could be unique to LlPC, taking into account its distinct biochemical and regulatory properties.

Binding Mode of c-di-AMP in LlPC. Clear electron density for c-di-AMP was observed from the crystallographic analysis (Fig. 3*A*). The c-di-AMP is bound at a solvent-exposed pocket at the CT dimer interface (Fig. 3*B*), 25 Å from the CT active site (Fig. 2*A*). The twofold axis of c-di-AMP aligns with that of the CT dimer (Fig. 3*B*), and there are two c-di-AMP molecules bound to the LlPC tetramer (Fig. 2*A*).

This is the equivalent c-di-AMP binding region as that in LmPC (6). However, the conformation of c-di-AMP and its interactions with the protein are significantly different between LmPC and LlPC (Fig. 3*C*). While c-di-AMP bound to LmPC adopts a U-shaped conformation, the c-di-AMP bound to LlPC is found in a somewhat more extended conformation (Fig. 3 *C* and *D*).

The Tyr715 residue in LlPC is equivalent to Tyr722 in LmPC and makes direct face-to-face π-stacking interactions with the adenine base (Fig. 3*C*). However, there is a difference in the position of the tyrosine side chain in LlPC, which is necessary to accommodate the more extended conformation of c-di-AMP (Fig. 3*C*). Tyr749 in LmPC makes a hydrogen bond with one terminal oxygen of the c-di-AMP phosphate group, and it also forms the base of the binding pocket (Fig. 3*C*). The residue is replaced by Ile742 in LlPC, and the c-di-AMP bound to LlPC sits deeper in the binding pocket compared with LmPC (Fig. 3*C*) and with a 7° rotation (Fig. 3*D*), likely due to the extra space provided by the Tyr749→Ile742 and Ala753→Gly746 substitutions in LlPC. The hydrogen bond to the c-di-AMP phosphate group is formed by Ser745 in LlPC instead (Ala752 in LmPC) (Fig. 3*C*). Ser745 also forms a water-mediated hydrogen bond with the ribose 2′-hydroxyl group. Finally, Ser756 in LmPC makes a water-mediated hydrogen bond with the other terminal oxygen of the c-di-AMP phosphate group. This residue is replaced with Gln749 in LlPC, which forms a direct hydrogen bond to this phosphate oxygen.

Mutagenesis and Biochemical Studies. To confirm the structural observations on the c-di-AMP binding site in LlPC, we introduced the Y715T mutation (making the residue identical to that in human PC; Fig. 1*B*). The mutant was expressed and purified using the same protocol as the WT protein. In LmPC, the equivalent mutation (Y722T) resulted in a greater than 50% loss in baseline catalytic activity (6). In comparison, the LlPC Y715T mutant had approximately the same baseline catalytic activity as the WT enzyme (Fig. 3*E*). As expected, the Y715T mutation abolished inhibition by c-di-AMP, confirming the c-di-AMP binding site identified in the crystal structure.

We also produced the G746A mutant (making the residue identical to that in EfPC), as the alanine side chain could have some clashes with the c-di-AMP ribose based on the structure

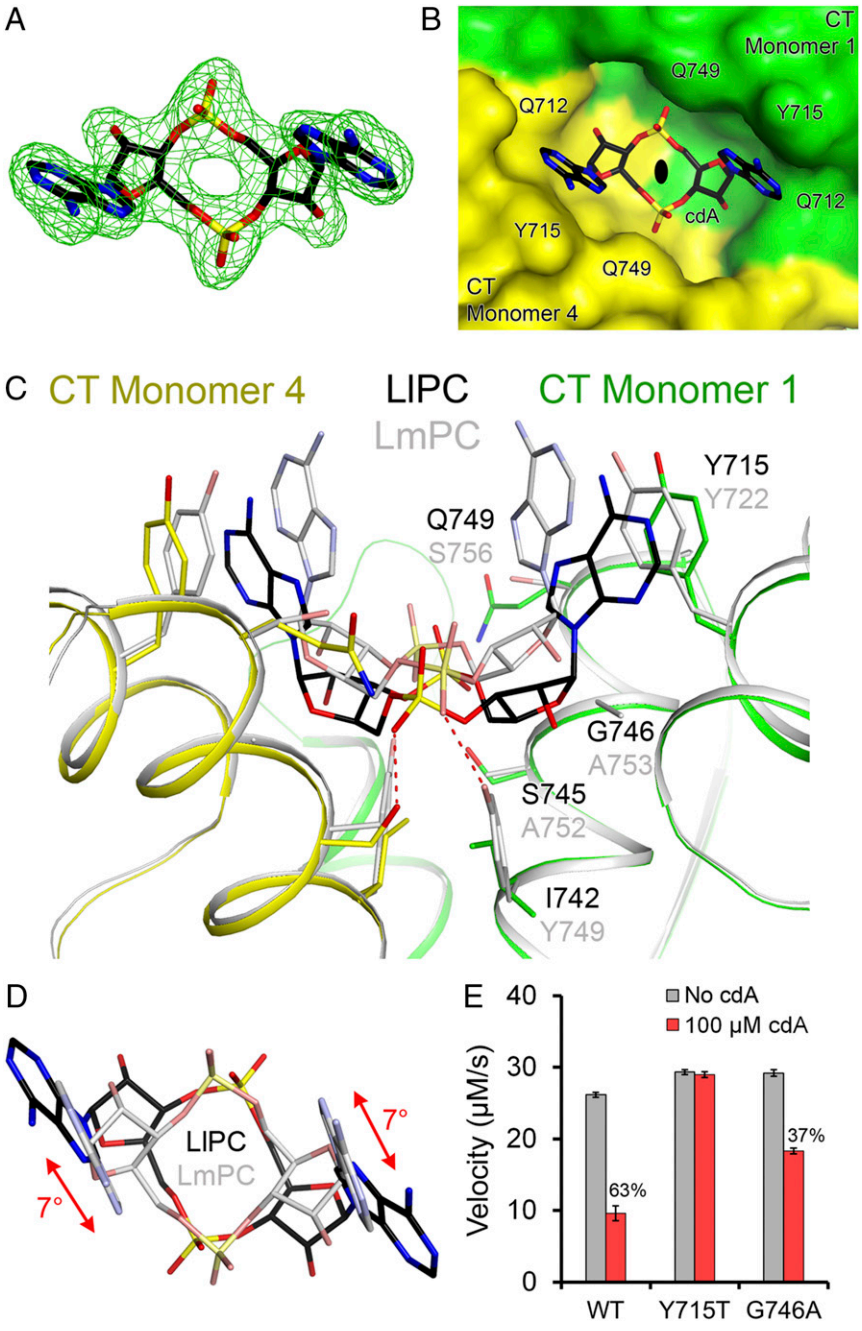

Fig. 3. Binding mode of c-di-AMP in LIPC. (*A*) Omit F_o–F_c electron density at 2.3-Å resolution for c-di-AMP, contoured at 3σ. (*B*) Molecular surface of LIPC near the c-di-AMP binding site. The compound is bound at the CT dimer interface, and the view is down the twofold axis of this dimer, indicated with the black oval. (*C*) Overlay of the binding mode of c-di-AMP (black) in LIPC (green and yellow) versus that in LmPC (gray). The labels for LIPC residues (black) are placed above those for the equivalent LmPC residues (gray). (*D*) Overlay of the bound conformations of c-di-AMP in LIPC (black) and LmPC (gray). The view is down the twofold axis of the CT dimers. There is a rotation of the central ring of c-di-AMP in the LIPC complex relative to that in the LmPC complex. (*E*) Kinetic data showing that the Y715T mutant is insensitive to c-di-AMP while the G746A mutant had reduced sensitivity. The percentage inhibition for WT LIPC and the mutants are indicated. The reactions contained 0.16 μM LIPC and 20 mM pyruvate. Error bars represent SDs over three separate experiments.

(2.2-Å distance). This mutant also had approximately the same baseline catalytic activity as WT, although the inhibition by c-di-AMP was reduced to 40% (Fig. 3*E*), lower than the 60% inhibition for the WT enzyme. We determined the crystal structure of the G746A mutant in complex with c-di-AMP at 2.0-Å resolution (Table S1). The overall structure of the G746A mutant tetramer is essentially identical to that of the WT protein (0.39-Å rms distance for their equivalent Cα atoms; Fig. S2). There are only minor conformational changes for c-di-AMP to fit into the new binding pocket (Fig. S2). This c-di-AMP binding mode to the G746A mutant may closely approximate that to EfPC, as the only remaining difference in the pocket is a Lys756 in EfPC instead of Gln749 in LIPC. Lys756 can maintain the same interaction with c-di-AMP as that observed for Gln749 (Fig. 3*C*).

Large Conformational Changes upon c-di-AMP Binding. We then determined the free LIPC structure, in the absence of c-di-AMP, at 3.1-Å resolution (Table S1). All four BCCP domains are disordered in this structure, although one ordered biotin is observed in the exo site, which was first identified in the SaPC structure (28). Three of the B subdomains of BC are disordered, while one B subdomain is in an open conformation with an empty BC active site.

The overall structure of free LIPC is remarkably different from that of the c-di-AMP complex (Fig. 4*A*). The BC dimers are farther apart from each other while the CT dimers move closer in the free LIPC tetramer, such that the free LIPC tetramer is more diamond-shaped while the c-di-AMP complex is square-shaped. The most apparent consequence of these conformational changes is that the PT domains in the free LIPC structure dimerize (Fig. 4*A*), as observed in SaPC and HsPC (28). This is in contrast to free LmPC, where the PT domains do not interact and in fact are even further apart than in the c-di-AMP complex (6). In free LIPC, the PT domain interaction is mediated primarily by hydrophobic

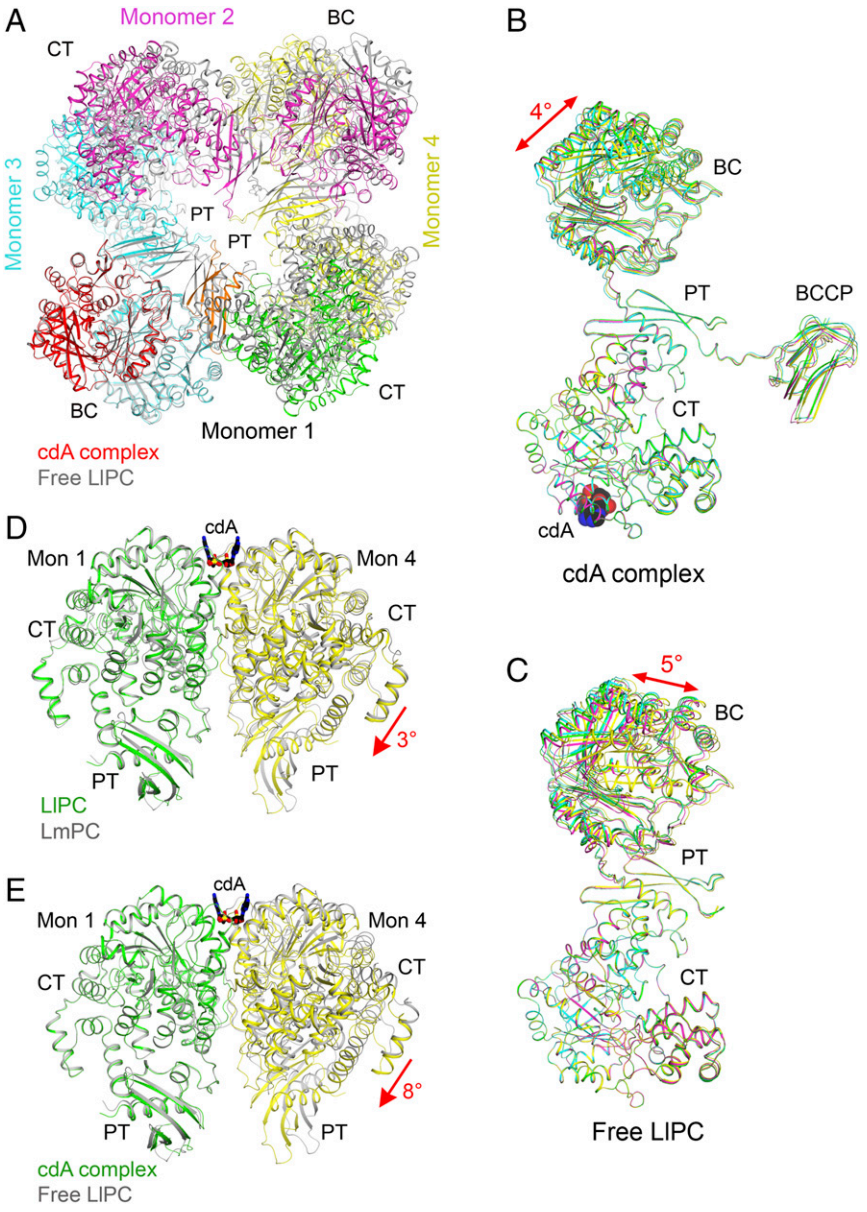

Fig. 4. Large conformational changes in LIPC upon c-di-AMP binding. (*A*) Overlay of the structures of the c-di-AMP complex (in color) and free enzyme (gray) of LIPC tetramer. The BC dimer of monomers 1 and 3 was used for the overlay. The BCCP domains in the c-di-AMP complex were removed for clarity. (*B*) Overlay of the four monomers in the c-di-AMP complex of LIPC by their CT domains. A small difference is observed for the BC and BCCP domains. (*C*) Overlay of the four monomers in the free enzyme of LIPC by their CT domains. The four monomers have roughly the same conformation as well. (*D*) Overlay of the LIPC CT dimer in the c-di-AMP complex (in color) with the LmPC CT dimer in the c-di-AMP complex (gray). The CT domain in monomer 1 was used for the overlay, but the overall structures of the two dimers are similar, with rms distance of 0.89 Å for their equivalent Cα atoms. (*E*) Overlay of the LIPC CT dimer in the c-di-AMP complex (in color) with that in the free enzyme (gray). A large difference for the CT domain in monomer 4 is seen, corresponding to a 5° rotation (red arrow).

interactions between Phe1036 of the two monomers. The equivalent residue in SaPC and HsPC (Phe1077) has previously been found to be critical for maintaining those tetramers as determined by gel filtration (28).

As observed for the LmPC c-di-AMP complex (6), the four monomers of the LIPC c-di-AMP complex have essentially the same conformation. With their CT domains in overlay, only small differences in the positions of the BC and BCCP domains are observed, corresponding to a 4° rotation (Fig. 4*B*). The conformations of the four monomers in the free LIPC structure are also similar (Fig. 4*C*), in sharp contrast to free LmPC where large differences are observed among the four monomers (6).

The BC dimer in the free and c-di-AMP–bound LIPC structures are similar (0.55-Å rms distance for their equivalent Cα atoms; Fig. S3), indicating that c-di-AMP does not affect the BC dimer conformation. On the other hand, a major conformational change of the CT dimer is observed between free LIPC and the c-di-AMP complex. In fact, the CT dimer in the LIPC c-di-AMP complex is more similar to that in the LmPC c-di-AMP complex (Fig. 4*D*) than the CT dimer from free LIPC (Fig. 4*E*). This indicates that c-di-AMP binding leads to a distinct CT dimer conformation. In addition, there is a significant change in the shape of the c-di-AMP binding pocket at the CT dimer interface between free LIPC and the c-di-AMP complex (Fig. S3). In particular, the side chains of Gln742 and Gln749 occlude the binding pocket in free LIPC and move to allow c-di-AMP binding.

By comparing the free LIPC tetramer to all previously determined PC structures, we found that the most similar was the SaPC structure in complex with CoA (Fig. S4; the acetyl-CoA used in that experiment was hydrolyzed to CoA during crystallization) (34). On the other hand, the free LIPC structure does not align as well with free SaPC (Fig. S4). Moreover, the BC dimer in the free LIPC structure is much more similar to the BC dimer in the SaPC–CoA complex (0.86 Å) than to the free SaPC structure (1.57 Å). Therefore, the LIPC tetramer appears to adopt an "acetyl-CoA–bound" conformation, even in the absence of the acetyl-CoA ligand. The four monomers of SaPC become more similar to each other upon CoA binding (28, 34), and in this regard LIPC appears to be more similar to SaPC than LmPC.

Molecular Basis for the Insensitivity of LIPC to Acetyl-CoA Activation. LIPC appears to be unique among single-chain PC enzymes as it

is essentially insensitive to activation by acetyl-CoA (Fig. 1*E*). The similarity of the free LlPC structure to the CoA complex of SaPC led us to investigate the possibility that there are specific sequence variations in LlPC that promote this activated tetramer conformation. Comparing the structure of the CoA complex to the free enzyme of SaPC, we noticed that CoA binding causes an increase in the interface area between the BC domain and the PT domain of the nearest monomer in the other layer of the tetramer (Fig. 5*A* and Fig. S5). This BC–PT interface region is also the location of acetyl-CoA binding (Fig. S5). The PT domain of free SaPC would clash with acetyl-CoA; thus, these conformational differences between free and CoA-bound SaPC are caused directly by acetyl-CoA binding.

In the free LlPC structure, this BC–PT interface shows a surface area burial actually larger than the CoA complex of SaPC (Fig. 5*A*). Sequence analysis among various PC homologs in this interface region revealed several residues that appear to be unique to LlPC (Fig. 5*B*), and which help to form contacts between the domains in the structure (Fig. 5*C*). Two residues in the PT domain (Lys1006 and Ser1018) are unique to LlPC among the sequences analyzed, while the two residues in the BC domain (Glu36 and Tyr37) are found in LlPC and EfPC only. By comparison, the residues at the BC dimer interface are well conserved between LlPC and other PC homologs. A quadruple mutant was designed to perturb the BC–PT interface in LlPC, in which these four residues were mutated to their equivalents in SaPC (E36K, Y37S, K1006T, and S1018I; Fig. 5*B*). This mutant LlPC exhibited a fourfold decrease in the k_{cat} compared with WT LlPC in the absence of acetyl-CoA, suggesting that the mutations have converted LlPC into a less active state. Moreover, this mutant LlPC is activated by acetyl-CoA by approximately twofold, with a K_a of ~10 μM (Fig. 5*D*). In comparison, SaPC is activated approximately sixfold by acetyl-CoA, with a K_a of 2 μM. Thus, these mutations cause the enzyme to become sensitive to acetyl-CoA, implicating this BC–PT interface as an important allosteric regulatory site for catalysis and activation by acetyl-CoA.

The Role of LlPC in Growth and Milk Acidification by *L. lactis*. Like most lactic acid bacteria, *L. lactis* contains a truncated TCA cycle (Fig. 6*A*). Amino acids aspartate and glutamate can be synthesized from the TCA intermediates oxaloacetate and α-ketoglutarate, respectively. However, in the case of *L. lactis*, glutamate is unable to be synthesized due to a lack of isocitrate dehydrogenase and glutamate dehydrogenase activities (35) (Fig. 6*A*). To determine whether LlPC is required for aspartate biosynthesis, we generated a markerless LlPC deleted mutant (Δ*pycA*) and tested its ability to grow in rich media (GM17) and chemically defined media (CDM). The Δ*pycA* strain grew similarly to WT in GM17, which contains abundant amino acids. The mutant was, however, unable to grow in CDM in the absence of either aspartate or asparagine (Fig. 6*B*). Complementation of the *pycA* gene (pGh9-*pycA*) into Δ*pycA* restored growth in CDM (Fig. 6*B*). Aspartate is the precursor of asparagine and their interconversion is likely carried out in *L. lactis* by AsnB and AnsB (36). These results demonstrate that LlPC is essential for oxaloacetate and ultimately aspartate biosynthesis in *L. lactis*.

Next, we examined whether LlPC is important for milk acidification, an important industrial property of *L. lactis*. Since the *L. lactis* strain MG1363 does not contain lactose uptake and utilization genes, cells were grown in milk supplemented with glucose. The acidification rate of the Δ*pycA* strain was significantly slower than the *pycA* complemented strain (Fig. 6*C*). The growth rate of Δ*pycA* (+pGh9) and Δ*pycA* (+pGh9-*pycA*) in glucose-supplemented milk were similar; however, Δ*pycA* (+pGh9-*pycA*) reached a higher late stationary-phase colony-forming units per milliliter ($P < 0.01$ at 18 h and $P < 0.001$ at 23 h). Accelerated milk acidification was observed when the complemented strain entered stationary phase, at which point cell numbers were indifferent to the mutant ($P = 0.39$ at 12 h and $P = 0.20$ at 14 h) (Fig. 6*C*). Therefore, we hypothesized that Δ*pycA* experiences aspartate deprivation near the stationary phase, which results in slower metabolism and poor milk acidification. To test this, different amino acids were supplemented into the milk media. The addition of aspartate or asparagine to milk fully restored acidification rates and stationary-phase cell numbers of the Δ*pycA* strain comparable to the WT (Fig. 6*D*). Together these results imply that LlPC is important for the supply of aspartate to achieve efficient acidification of milk by *L. lactis*.

Regulation of Aspartate Biosynthesis by c-di-AMP Control of LlPC. We hypothesized that aspartate biosynthesis in *L. lactis* is regulated

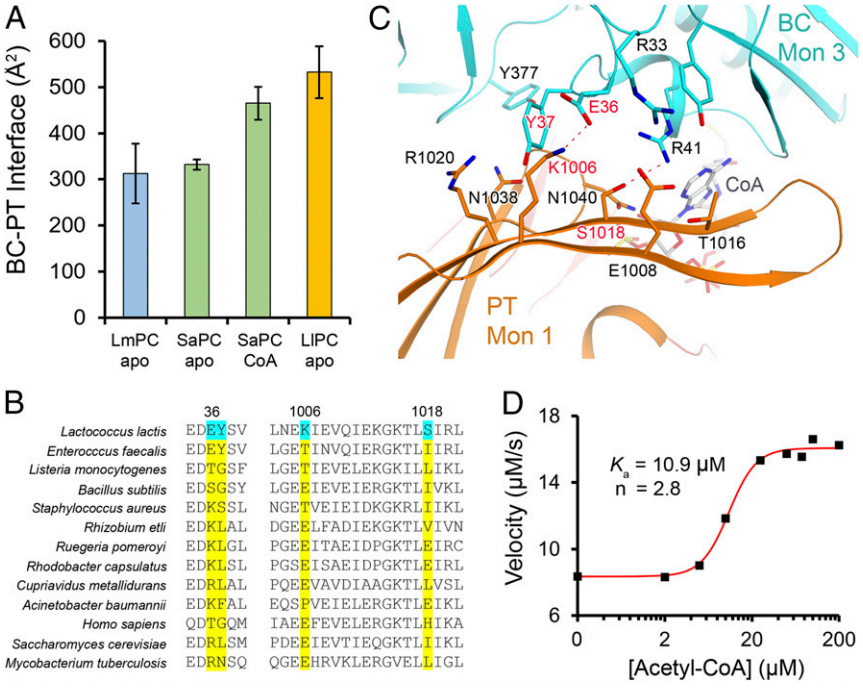

Fig. 5. Molecular basis for LlPC insensitivity to acetyl-CoA activation. (*A*) Surface area burial at the BC–PT interface in the structures of LmPC c-di-AMP complex, SaPC free enzyme, SaPC CoA complex, and LlPC c-di-AMP complex. (*B*) Sequence alignment of residues in the BC–PT interface. Four residues that are unique to LlPC are highlighted in cyan. (*C*) Detailed interactions at the BC–PT interface, with the four residues that are unique to LlPC labeled in red. (*D*) The quadruple mutant of LlPC is sensitive to acetyl-CoA and is activated by about twofold. The reactions contained 0.4 μM of the mutant protein and 10 mM pyruvate.

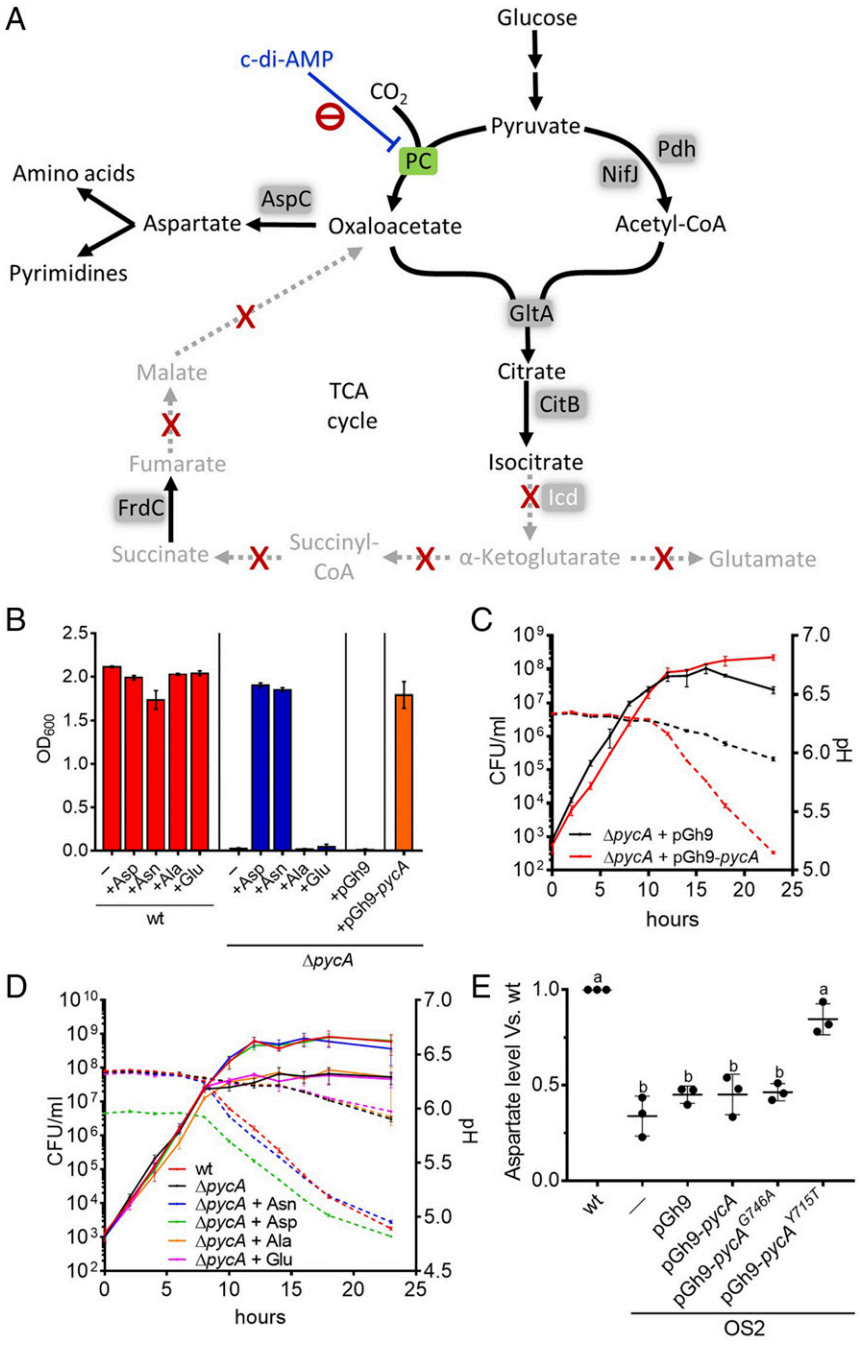

Fig. 6. The role of LlPC in growth and milk acidification in *Lactococcus* and c-di-AMP–regulated aspartate biosynthesis. (*A*) Schematic diagram of *L. lactis* central metabolism and truncated TCA cycle. Solid lines indicate enzymatic steps present in *L. lactis*, while dotted lines with a red "x" indicate the enzyme is missing. For Icd, the gene is present, but enzymatic activity is absent in *L. lactis*. Metabolites written in gray are not formed in this metabolic pathway. (*B*) Growth of *L. lactis* strains in CDM with or without amino acid supplementation after 20-h incubation. (*C*) Growth (solid lines) and acidification (dotted lines) of milk supplemented with glucose. (*D*) Growth (solid lines) and acidification (dotted lines) of milk supplemented with glucose with or without additional amino acids. Note that aspartate addition slightly lowers the milk pH. (*E*) Intracellular aspartate levels in WT, the high c-di-AMP *gdpP* mutant strain OS2, and OS2 strain containing plasmids with or without WT or mutated *pycA*. Different letters indicate statistically significant differences at $P < 0.0001$ (Tukey's multiple-comparisons test). Data presented in *B*–*E* are mean ± SD from three independent biological replicates.

by c-di-AMP binding to LlPC. The intracellular levels of aspartate in WT and a high c-di-AMP *gdpP* mutant strain (OS2) (2) were measured. The aspartate level in OS2 was 65% lower compared with WT (Fig. 6*E*), suggesting that high c-di-AMP dampens aspartate synthesis. To determine whether this lower aspartate level is due to c-di-AMP–mediated inhibition of LlPC, we introduced into strain OS2 genes encoding WT LlPC as well as the G746A and Y715T mutants, which are partially or completely insensitive to c-di-AMP, respectively (Fig. 3*E*). The aspartate level in OS2 overexpressing $pycA^{G746A}$ was insignificantly different to OS2 only, OS2 containing an empty plasmid, or OS2 overexpressing WT *pycA* (Fig. 6*E*). Overexpression of $pycA^{Y715T}$ in OS2, however, resulted in restoration of aspartate levels comparable to WT (Fig. 6*E*). Therefore, only the completely insensitive LlPC Y715T mutant was able to restore aspartate levels in a high c-di-AMP *L. lactis* strain. The inability of the $pycA^{G746A}$-expressing strain to partially elevate aspartate levels may be due to the presence of background WT LlPC expressed from the genome in these strains resulting in PC heterotetramers that could exhibit greater sensitivity toward c-di-AMP, or the difference between in vivo and in vitro assay conditions. Nonetheless, these findings demonstrate that c-di-AMP–mediated regulation of LlPC function is important for modulating the aspartate pool in *L. lactis*.

Discussion

Similar to *L. monocytogenes*, *L. lactis* lacks the α-ketoglutarate dehydrogenase enzyme and has a truncated TCA cycle. The oxaloacetate generated by PC can be diverted into three pathways: (*i*) the oxidative pathway leading in a few steps to α-ketoglutarate and NADH; (*ii*) the reductive pathway leading to malate and then succinate; and (*iii*) the biosynthesis of

aspartate through aspartate aminotransferase (37). However, unlike *L. monocytogenes*, *L. lactis* lacks the glutamate dehydrogenase enzyme to convert α-ketoglutarate to glutamate, and glutamate cannot be produced de novo (38). In addition, the upstream enzyme isocitrate dehydrogenase, which converts isocitrate to α-ketoglutarate, has also been found to be nonfunctional (35), although its activity has been detected in one atypical *L. lactis* strain (37). Thus, compared with *L. monocytogenes* in which production of glutamate is one of the main functions of PC activity (6), this oxidative pathway may be less important in *L. lactis*.

Instead, the primary function of PC activity in *L. lactis* appears to be aspartate biosynthesis based on our work here and that of others. Early studies involving [^{14}C]bicarbonate feeding found that the major product of CO_2 fixation in *L. lactis* cells was aspartate, with 90% of the radiolabel incorporated into this one amino acid (39). In agreement with this, aspartate was found to be the only significant de novo-synthesized amino acid in *L. lactis*, with all other amino acids being taken up mostly from the medium (40). With regards to its role in *L. lactis*, a slow milk coagulation phenotype (Fmc$^-$) in *L. lactis* was found to be caused by a deficiency in PC, and this defect could be rescued by supplementing the growth medium with aspartate or aspartate-containing peptides (41). This strain, however, was created using chemical mutagenesis, and although the level of PC protein was found to be lower, the nature of the mutation(s) in this strain is as yet unknown (27). The single aspartate aminotransferase AspC in *L. lactis*, which converts oxaloacetate to aspartate, has also been found to be essential for growth in minimal media and milk acidification (42). It was mentioned that the *aspC* mutant was unable to grow in milk; however, this was determined by measuring OD_{600} levels using a milk clarification procedure, not viable cells counts (42). Like that observed here for Δ*pycA*, it is therefore possible that the *aspC* mutant can grow in milk, but to lower final cell densities, which can be difficult to observe following milk clarification. Although aspartate is abundant in the major milk protein casein, it is clear that de novo synthesis via PC and AspC is necessary to achieve efficient acidification.

Aspartate is a precursor for several other amino acids as well as for pyrimidine biosynthesis. Changes in the aspartate pool in *L. lactis* will likely have significant implications for downstream biosynthetic pathways, which contribute to phenotypes controlled by c-di-AMP. For example, recent work has suggested that the aspartate pool affects cell wall cross-linking and peptidoglycan plasticity in *L. lactis*, since it is a precursor for peptidoglycan cross-bridge amino acids (43). One of the best-characterized roles of c-di-AMP is in osmoregulation where it controls the two primary mechanisms that bacteria use to deal with changes in osmotic pressure—solute uptake and cell wall strength. c-di-AMP binds to and negatively regulates potassium (9, 44) and compatible solute transporters (7, 8) and also affects peptidoglycan precursor biosynthesis (2). Recent work has identified suppressor mutations in osmoprotectant transporters as well as in PC in a Δ*dacA* mutant of *L. monocytogenes* (26). This study suggested that PC-controlled metabolic products play a role in osmoregulation, which would explain why c-di-AMP targets an enzyme involved in central metabolism.

The characteristics of *L. lactis* suggest that the unique biochemical properties of LlPC have been adapted for the particular growth requirements of the bacterium. Acetyl-CoA regulation of PC couples the levels of acetyl-CoA in the cell to the production of oxaloacetate by PC, such that citrate synthase can efficiently convert acetyl-CoA and oxaloacetate to citrate. This metabolic pathway appears to be less important in *L. lactis*, while the conversion of oxaloacetate to aspartate is prioritized. This prioritization of aspartate biosynthesis over citrate is consistent with our finding that LlPC is not subject to acetyl-CoA regulation as is observed in other PC enzymes. In addition, LlPC has a much higher k_{cat} than previously studied PC enzymes, suggesting that high levels of PC activity are needed to sustain bacterial growth. In *L. lactis*, c-di-AMP is used as a negative allosteric regulator to dampen the high baseline enzymatic activity of PC. In other bacterial species that do not use c-di-AMP to regulate PC, the opposite may be the case, where PC activity is low at baseline, and acetyl-CoA is used to up-regulate activity as needed. *L. monocytogenes* appears to have the most complex regulation, with both c-di-AMP and acetyl-CoA working in concert to modulate enzymatic activity. This dual regulation in *L. monocytogenes* may be necessary to meet specific metabolic demands, while less fine-tuned regulation may be adequate in other bacterial species.

LlPC has acquired several mutations at the BC–PT interface in the tetramer, which is also the location for acetyl-CoA binding as identified in RePC and SaPC. Structurally, these mutations result in greater surface area burial in the BC–PT interface in LlPC, similar to that observed in the CoA complex of SaPC. The BC dimer conformation as well as the overall tetramer structure of LlPC are also similar to the CoA complex of SaPC. Biochemically, these mutations result in a more active enzyme, which no longer responds to acetyl-CoA activation. As a result, regulation by c-di-AMP appears to be the main control mechanism for LlPC activity. However, LlPC still contains an intact acetyl-CoA binding pocket and is activated by acetyl-CoA to a small degree when it is in an inhibited state bound to c-di-AMP. Thus, LlPC appears to be regulated in opposing directions by both c-di-AMP and acetyl-CoA, which is similar to that for LmPC.

The LlPC and LmPC structures indicate that c-di-AMP can be recognized even without strict conservation of the binding pocket. The divergent amino acids interacting with c-di-AMP result in distinct conformations of the compound to fit the particular shape of the binding pocket. Like in LmPC, the adenine does not appear to be recognized specifically by LlPC, so how the specificity for c-di-AMP over c-di-GMP is achieved remains unclear. These structures suggest that the minimum requirements for c-di-AMP binding to PC include an aromatic residue to π-stack with the adenine, and small residues (serine, alanine, glycine) at positions 745–746 (752–753 in LmPC) in order for c-di-AMP to gain access to the pocket. These rules can be used to identify other bacterial PCs, which are regulated by c-di-AMP. The LmPC and LlPC structures demonstrate that even divergent residues in the binding pocket can recognize c-di-AMP, and other bacterial PCs could recognize c-di-AMP using yet other sets of residues.

Even with the differences in how LmPC and LlPC recognize c-di-AMP, in both cases the compound appears to act as a sort of molecular wedge, in which the CT monomers are pushed apart to adopt a particular "c-di-AMP–bound" CT dimer conformation. This change in the shape of the CT dimer leads to a dramatic change in the overall tetramer conformation in both LmPC and LlPC. This local change in the CT dimer conformation and/or the global change in the tetramer may be the molecular mechanism for the inhibitory effect of c-di-AMP. It has been proposed that acetyl-CoA activates PC activity by changing the BC dimer to a more active conformation (34). A similar mechanism could also be possible for the CT dimer, although how the observed structural changes would result in the inhibition of the CT active site is not clear. Another possibility is that the overall tetramer conformation induced by c-di-AMP may restrict movement of BCCP between the active sites or its access to the active sites.

Methods

Protein Expression and Purification. The *Lactococcus lactis* strain was obtained from the US Department of Agriculture Agricultural Research Service Culture Collection from which the genomic DNA was purified. The pyruvate carboxylase gene for *Lactococcus lactis* was amplified from genomic DNA and subcloned into the pET28a vector with an N-terminal hexahistidine tag (Novagen). This expression construct was then cotransformed into BL21 Star (DE3) cells along with a plasmid encoding the *Escherichia coli* biotin ligase (*BirA*) gene.

The cells were cultured in LB medium with 35 mg/L kanamycin and 35 mg/L chloramphenicol and were induced for 14 h with 1 mM IPTG at 20 °C. Before induction, 20 mg/L biotin and 10 mM $MnCl_2$ were supplemented to the

culture medium. The protein was purified through nickel-agarose affinity chromatography (Qiagen) followed by gel filtration chromatography (Sephacryl S-300; GE Healthcare). The purified protein was concentrated to 15 mg/mL in a buffer containing 20 mM Tris (pH 8.0), 150 mM NaCl, 5% (vol/vol) glycerol, and 5 mM DTT, flash-frozen in liquid nitrogen, and stored at –80 °C. The protein was confirmed to be fully biotinylated by a streptavidin gel-shift assay. Streptavidin was added in a 2:1 molar ratio to the protein before running the sample on the gel. The complex with biotin is stable to the presence of SDS and causes a shift of the protein band. The N-terminal hexahistidine tag was not removed for crystallization.

Protein Crystallization. Crystals of LlPC were grown by the sitting-drop vapor diffusion method at 20 °C. For the c-di-AMP complex, the protein at 5 mg/mL was incubated with 2.5 mM c-di-AMP and 2.5 mM ATP for 30 min at 4 °C before crystallization setup. The reservoir solution contained 20% (wt/vol) PEG3350, and 0.2 M ammonium formate. Crystals appeared within a few days and grew to full-size within 1 wk. The crystals were cryoprotected in the reservoir solution supplemented with 18% (vol/vol) ethylene glycol and were flash-frozen in liquid nitrogen for data collection at 100 K.

For LlPC free enzyme, the protein at 5 mg/mL was incubated with 4 mM ATP for 30 min at 4 °C before crystallization setup. The reservoir solution contained 15% (wt/vol) PEG 3350 and 0.2 M ammonium tartrate. Crystals appeared after 2 d and grew to full-size within a week. They were cryoprotected in the reservoir solution supplemented with 25% (vol/vol) ethylene glycol and flash-frozen in liquid nitrogen for data collection at 100 K.

Data Collection and Structure Determination. X-ray diffraction data were collected at the Advanced Photon Source beamline NE-CAT 24-ID-C using a Pilatus-6MF detector. The diffraction images for the c-di-AMP complex were processed using HKL2000 (45). The diffraction images for the free enzyme were processed using XDS (46), and scaled with the program Aimless in the CCP4 package (47).

The structures were solved by the molecular replacement method with the program Phaser (48), using the BC, CT, and BCCP domains of the *Listeria monocytogenes* PC structure as the search models. Manual rebuilding was carried out with Coot (49) and refinement with the program Refmac (50).

Mutagenesis and Kinetic Studies. Mutants were made using the QuikChange kit (Stratagene) and confirmed by sequencing. They were expressed and purified following the same protocol as described for the WT enzyme. The catalytic activity was determined based on a published protocol (51), which couples oxaloacetate production to the oxidation of NADH by malate dehydrogenase, followed spectrophotometrically by the decrease in absorbance at 340 nm. The activity was measured at room temperature in a reaction mixture containing 20 mM Tris (pH 7.5), 200 mM NaCl, 5 mM $MgCl_2$, 50 mM sodium bicarbonate, 50 mM ammonium sulfate, 5 units of malate dehydrogenase (Sigma), 2 mM ATP, and pyruvate carboxylase and pyruvate concentrations as stated. The k_{cat} was calculated based on PC monomers.

Bacterial Culture Conditions. *L. lactis* strains (Table S2) were grown at 30 °C in M17 media (Difco) (52) supplemented with 0.5% (wt/vol) glucose (GM17). *L. lactis* pRV300 derivatives or *L. lactis* with freely replicating pGh9 were grown at 30 °C in the presence of 3 μg/mL erythromycin (Em). *E. coli* NEB-5α containing pRV300 derivatives were grown in Luria–Bertani broth (LB) containing 100 μg/mL ampicillin at 37 °C with aeration at 230 rpm (OM11 Orbital mixer, Ratek). *E. coli* NEB-5α containing pGh9 derivatives were grown in Heart Infusion media (Oxoid) containing 150 μg/mL Em at 30 °C with aeration at 230 rpm (OM11 Orbital mixer, Ratek).

Construction of a Δ*pycA* Mutant and *pycA* Complemented *L. lactis* Strains. Primers and plasmids used in this study are shown in Tables S3 and S4. A Δ*pycA* mutant strain was generated using a two-step single crossover homologous recombination process with the nonreplicating plasmid pRV300. DNA fragments (~1 kb) upstream and downstream of *pycA* (*llmg_0643*) were joined via overlap extension PCR (OE-PCR). A small amount (40 bp from the start and 65 bp from the end) of *pycA* was included in the fragments to limit disruption of upstream and downstream genes. The joined DNA was ligated into XhoI- and PstI-digested pRV300. The plasmid was transformed into *E. coli* NEB-5α, verified by sequencing, and electroporated into *L. lactis* MG1363 using a previously described method (53). A single recombinant was selected on GM17 media containing 3 μg/mL Em (GM17Em) and plasmid integration confirmed by PCR. The plasmid was then removed from the chromosome by successive subculturing in GM17 broth supplemented with L-asparagine (0.125 g/L) but without erythromycin (GM17-Asn). Asparagine was added in case the Δ*pycA* strain possessed a growth defect due to low asparagine/aspartate levels. To identify plasmid excision, colonies were replica plated onto GM17-Asn with and without Em. PCR was used to confirm deletion of *pycA* in Em-sensitive colonies. For complementation, the entire *pycA* gene was cloned into PstI- and XhoI-digested pGh9. The pGh9 plasmid is derived from pGh9::IS*1* (54), which contains an Em resistance gene upstream of the PstI site. The lack of a transcription terminator after the Em gene likely allows for expression of the downstream cloned *pycA* gene. The plasmid was transformed into *E. coli* NEB-5α, verified by sequencing, and electroporated into the Δ*pycA* mutant.

Construction of *pycA*-, *pycA*^{Y715T}-, and *pycA*^{G746A}-Overexpressing Strains. OE-PCR was used to generate *pycA*^{Y715T} and *pycA*^{G746A} mutations by the fusing of two ~1.5-kb DNA fragments. These joined fragments were ligated into XhoI- and PstI-digested pRV300, and the plasmids were verified by sequencing after transforming into *E. coli* NEB-5α. They were integrated into *L. lactis* MG1363 and the *gdpP* mutant OS2 using the same two-step single-crossover homologous recombination process as above, except L-asparagine was not supplemented into the media. Strains containing the *pycA*^{Y715T} and *pycA*^{G746A} were obtained and confirmed by PCR and sequencing. However, we noticed that, in strain OS2, osmoresistant suppressor mutations frequently occurred during subculturing over several days in the plasmid excision step. Therefore, the complete mutated *pycA* genes were instead amplified from MG1363 containing *pycA*^{Y715T} and *pycA*^{G746A} in the chromosome and cloned into PstI- and XhoI-digested pGh9 and electroporated into *L. lactis* OS2 along with the pGh9-*pycA* plasmid.

Growth in Chemically Defined Media. The chemically defined medium (CDM) was prepared by supplementing important components for growth of *Lactococcus* (55) into Dulbecco's modified Eagle's medium (DMEM) (Sigma-Aldrich; catalog no. D5921). Additional components were provided as indicated: 0.011 g/L adenine, 0.001 g/L guanine, 0.0038 g/L xanthine, 0.023 g/L uracil, 3.6 g/L KH_2PO_4, 7.3 g/L K_2HPO_4, 13.05 g/L Mops, 0.13 g/L L-histidine, 0.72 g/L L-arginine, 1 g/L L-leucine, 0.6 g/L L-valine, 0.584 g/L L-glutamine, 0.9 g/L potassium acetate, 0.006 g/L biotin, 0.0075 g/L EDTA, 0.004 g/L $FeSO_4{\cdot}7H_2O$, 0.005 g/L $ZnSO_4{\cdot}7H_2O$, 0.00038 g/L $MnSO_4.4H_2O$, and 5 g/L glucose. When required, CDM was supplemented with 0.125 g/L L-asparagine, 0.42 g/L L-aspartate, 0.1 g/L L-glutamate, 0.24 g/L L-alanine, or 3 μg/mL Em. *L. lactis* strains were grown in GM17 at 30 °C overnight with or without Em as required. Overnight cultures were then diluted 1:100 in fresh GM17 media with or without Em until midexponential phase (OD_{600} of ~0.6). Aliquots (1.5 mL) were centrifuged and resuspended in 1 mL of DMEM, and then between 100 and 200 μL was used to inoculate CDM. Cultures were incubated at 30 °C, and OD_{600} was determined after 20 h of incubation using a spectrophotometer (Lovibond). Averages and SDs were calculated based on three biological replicates.

Growth and Acidification in Skim Milk. Cultures were grown in GM17 with or without Em as required until an OD_{600} ~0.1. A 1- to 2-mL aliquot of cells was harvested by centrifugation (8,000 × *g*, 5 min) and washed and resuspended in 1 mL of 0.085% sterile NaCl. Cells were diluted a further 10-fold and 5 μL was added to 50 mL of 10% (vol/vol) sterile skim milk (Difco) containing 1% (wt/vol) glucose. Glucose was added since *L. lactis* MG1363 does not contain lactose utilization genes. When required, the skim milk was supplemented with 0.125 g/L L-asparagine, 0.42 g/L L-aspartate, 0.1 g/L L-glutamate, 0.24 g/L L-alanine, or 3 μg/mL erythromycin for plasmid-containing cells. Colony-forming units per milliliter were monitored by plating dilutions onto GM17 (with or without Em), and pH was measured using a standard benchtop pH meter (pH Cube; TPS). Averages and SDs were calculated based on three biological replicates, and statistical analysis was carried out using Tukey's multiple-comparisons test.

Extraction and Quantification of Aspartate. *L. lactis* was grown in GM17 broth with or without Em as required until OD_{600} ~0.8. Cells (20 mL) were pelleted by centrifugation at 5,000 × *g* for 10 min and washed twice with 2 mL of 0.01 M phosphate buffer (pH 7). Cells were then resuspended in 1.7 mL of deionized water and mixed with 0.5-mL equivalent of 0.1-mm zirconia/silica beads and disrupted using a Precellys 24 homogenizer (Bertin Technologies) three times for 1 min each, with 1-min cooling on ice in between. Glass beads were separated by centrifugation at 21,380 × *g* for 5 min, and then supernatants were collected. Relative lysis efficiency was determined by OD_{280} using a NanoDrop One (Thermo Scientific). Aspartate was quantified using an aspartate assay kit (MAK095; Sigma-Aldrich). In this method, aspartate is converted to pyruvate, which is then oxidized by a probe that changes color (OD_{570}). Reaction mixes for samples consisted of 0.5 μL of aspartate enzyme mix, 0.5 μL of conversion

mix, and 0.5 μL of probe, and were adjusted to 12.5 μL with aspartate assay buffer. Reaction mixes for the background control (to correct for pyruvate present in the sample) were set up the same as for samples, but omitting the aspartate enzyme mix. Cell extracts (4 μL) were adjusted to 12.5 μL with aspartate assay buffer and were added to each of the control and sample reaction mixes (total volume, 25 μL). Concentrations were calculated by subtracting the OD_{570} of the blank from the sample and dividing the obtained value by OD_{280}. Averages and SDs were calculated based on three biological replicates.

ACKNOWLEDGMENTS. We thank S. Banerjee, K. Perry, R. Rajashankar, J. Schuermann, and N. Sukumar for access to NE-CAT 24-C and 24-E beamlines at the Advanced Photon Source. This research was supported by Grants R01AI116669 (to J.J.W. and L.T.) and S10OD012018 (to L.T.) from the NIH and Grant LP120100282 (to M.S.T.) from the Australian Research Council. P.H.C. was also supported by an NIH Medical Scientist Training Program (GM007367). This work used Northeastern Collaborative Access Team beamlines (NIH Grant GM103403) and a Pilatus detector (NIH Grant RR029205) at the Advanced Photon Source (United States Department of Energy Grant DE-AC02-06CH11357).

1. Witte CE, et al. (2013) Cyclic di-AMP is critical for *Listeria monocytogenes* growth, cell wall homeostasis, and establishment of infection. *MBio* 4:e00282-13.
2. Zhu Y, et al. (2016) Cyclic-di-AMP synthesis by the diadenylate cyclase CdaA is modulated by the peptidoglycan biosynthesis enzyme GlmM in *Lactococcus lactis*. *Mol Microbiol* 99:1015–1027.
3. Luo Y, Helmann JD (2012) Analysis of the role of *Bacillus subtilis* σ^M in β-lactam resistance reveals an essential role for c-di-AMP in peptidoglycan homeostasis. *Mol Microbiol* 83:623–639.
4. Peng X, Zhang Y, Bai G, Zhou X, Wu H (2016) Cyclic di-AMP mediates biofilm formation. *Mol Microbiol* 99:945–959.
5. Gundlach J, Rath H, Herzberg C, Mäder U, Stülke J (2016) Second messenger signaling in *Bacillus subtilis*: Accumulation of cyclic di-AMP inhibits biofilm formation. *Front Microbiol* 7:804.
6. Sureka K, et al. (2014) The cyclic dinucleotide c-di-AMP is an allosteric regulator of metabolic enzyme function. *Cell* 158:1389–1401.
7. Huynh TN, et al. (2016) Cyclic di-AMP targets the cystathionine beta-synthase domain of the osmolyte transporter OpuC. *Mol Microbiol* 102:233–243.
8. Schuster CF, et al. (2016) The second messenger c-di-AMP inhibits the osmolyte uptake system OpuC in *Staphylococcus aureus*. *Sci Signal* 9:ra81.
9. Bai Y, et al. (2014) Cyclic di-AMP impairs potassium uptake mediated by a cyclic di-AMP binding protein in *Streptococcus pneumoniae*. *J Bacteriol* 196:614–623.
10. Dey B, et al. (2015) A bacterial cyclic dinucleotide activates the cytosolic surveillance pathway and mediates innate resistance to tuberculosis. *Nat Med* 21:401–406.
11. Yang J, et al. (2014) Deletion of the cyclic di-AMP phosphodiesterase gene (*cnpB*) in *Mycobacterium tuberculosis* leads to reduced virulence in a mouse model of infection. *Mol Microbiol* 93:65–79.
12. Bai Y, et al. (2013) Two DHH subfamily 1 proteins in *Streptococcus pneumoniae* possess cyclic di-AMP phosphodiesterase activity and affect bacterial growth and virulence. *J Bacteriol* 195:5123–5132.
13. Ye M, et al. (2014) DhhP, a cyclic di-AMP phosphodiesterase of *Borrelia burgdorferi*, is essential for cell growth and virulence. *Infect Immun* 82:1840–1849.
14. Corrigan RM, Gründling A (2013) Cyclic di-AMP: Another second messenger enters the fray. *Nat Rev Microbiol* 11:513–524.
15. Huynh TN, et al. (2015) An HD-domain phosphodiesterase mediates cooperative hydrolysis of c-di-AMP to affect bacterial growth and virulence. *Proc Natl Acad Sci USA* 112:E747–E756.
16. Kim H, et al. (2015) Structural studies of potassium transport protein KtrA regulator of conductance of K^+ (RCK) C domain in complex with cyclic diadenosine monophosphate (c-di-AMP). *J Biol Chem* 290:16393–16402.
17. Chin KH, et al. (2015) Structural insights into the distinct binding mode of cyclic di-AMP with SaCpaA_RCK. *Biochemistry* 54:4936–4951.
18. Choi PH, Sureka K, Woodward JJ, Tong L (2015) Molecular basis for the recognition of cyclic-di-AMP by PstA, a PII-like signal transduction protein. *MicrobiologyOpen* 4: 361–374.
19. Gundlach J, et al. (2015) Identification, characterization, and structure analysis of the cyclic di-AMP-binding PII-like signal transduction protein DarA. *J Biol Chem* 290: 3069–3080.
20. Campeotto I, Zhang Y, Mladenov MG, Freemont PS, Gründling A (2015) Complex structure and biochemical characterization of the *Staphylococcus aureus* cyclic diadenylate monophosphate (c-di-AMP)-binding protein PstA, the founding member of a new signal transduction protein family. *J Biol Chem* 290:2888–2901.
21. Müller M, Hopfner K-P, Witte G (2015) c-di-AMP recognition by *Staphylococcus aureus* PstA. *FEBS Lett* 589:45–51.
22. Jitrapakdee S, et al. (2008) Structure, mechanism and regulation of pyruvate carboxylase. *Biochem J* 413:369–387.
23. Tong L (2013) Structure and function of biotin-dependent carboxylases. *Cell Mol Life Sci* 70:863–891.
24. Choi PH, et al. (2016) A distinct holoenzyme organization for two-subunit pyruvate carboxylase. *Nat Commun* 7:12713.
25. Schär J, et al. (2010) Pyruvate carboxylase plays a crucial role in carbon metabolism of extra- and intracellularly replicating *Listeria monocytogenes*. *J Bacteriol* 192: 1774–1784.
26. Whiteley AT, et al. (2017) c-di-AMP modulates *Listeria monocytogenes* central metabolism to regulate growth, antibiotic resistance and osmoregulation. *Mol Microbiol* 104:212–233.
27. Wang H, O'Sullivan DJ, Baldwin KA, McKay LL (2000) Cloning, sequencing, and expression of the pyruvate carboxylase gene in *Lactococcus lactis* subsp. *lactis* C2. *Appl Environ Microbiol* 66:1223–1227.
28. Xiang S, Tong L (2008) Crystal structures of human and *Staphylococcus aureus* pyruvate carboxylase and molecular insights into the carboxyltransfer reaction. *Nat Struct Mol Biol* 15:295–302.
29. Adina-Zada A, Zeczycki TN, Attwood PV (2012) Regulation of the structure and activity of pyruvate carboxylase by acetyl CoA. *Arch Biochem Biophys* 519:118–130.
30. Yu LPC, Chou C-Y, Choi PH, Tong L (2013) Characterizing the importance of the biotin carboxylase domain dimer for *Staphylococcus aureus* pyruvate carboxylase catalysis. *Biochemistry* 52:488–496.
31. St Maurice M, et al. (2007) Domain architecture of pyruvate carboxylase, a biotin-dependent multifunctional enzyme. *Science* 317:1076–1079.
32. Lasso G, et al. (2010) Cryo-EM analysis reveals new insights into the mechanism of action of pyruvate carboxylase. *Structure* 18:1300–1310.
33. Lasso G, et al. (2014) Functional conformations for pyruvate carboxylase during catalysis explored by cryoelectron microscopy. *Structure* 22:911–922.
34. Yu LPC, Kim YS, Tong L (2010) Mechanism for the inhibition of the carboxyltransferase domain of acetyl-coenzyme A carboxylase by pinoxaden. *Proc Natl Acad Sci USA* 107:22072–22077.
35. Wang H, Baldwin KA, O'Sullivan DJ, McKay LL (2000) Identification of a gene cluster encoding Krebs cycle oxidative enzymes linked to the pyruvate carboxylase gene in *Lactococcus lactis* ssp. *lactis* C2. *J Dairy Sci* 83:1912–1918.
36. Veiga P, et al. (2009) Identification of the asparagine synthase responsible for D-Asp amidation in the *Lactococcus lactis* peptidoglycan interpeptide crossbridge. *J Bacteriol* 191:3752–3757.
37. Lapujade P, Cocaign-Bousquet M, Loubiere P (1998) Glutamate biosynthesis in *Lactococcus lactis* subsp. *lactis* NCDO 2118. *Appl Environ Microbiol* 64:2485–2489.
38. Jensen PR, Hammer K (1993) Minimal requirements for exponential growth of *Lactococcus lactis*. *Appl Environ Microbiol* 59:4363–4366.
39. Hillier AJ, Jago GR (1978) Metabolism of [^{14}C]bicarbonate by *Streptococcus lactis*: Identification and distribution of labeled compounds. *J Dairy Res* 45:231–240.
40. Jensen NB, Christensen B, Nielsen J, Villadsen J (2002) The simultaneous biosynthesis and uptake of amino acids by *Lactococcus lactis* studied by ^{13}C-labeling experiments. *Biotechnol Bioeng* 78:11–16.
41. Wang H, Yu W, Coolbear T, O'Sullivan D, McKay LL (1998) A deficiency in aspartate biosynthesis in *Lactococcus lactis* subsp. *lactis* C2 causes slow milk coagulation. *Appl Environ Microbiol* 64:1673–1679.
42. Dudley E, Steele J (2001) *Lactococcus lactis* LM0230 contains a single aminotransferase involved in aspartate biosynthesis, which is essential for growth in milk. *Microbiology* 147:215–224.
43. Solopova A, et al. (2016) Regulation of cell wall plasticity by nucleotide metabolism in *Lactococcus lactis*. *J Biol Chem* 291:11323–11336.
44. Corrigan RM, et al. (2013) Systematic identification of conserved bacterial c-di-AMP receptor proteins. *Proc Natl Acad Sci USA* 110:9084–9089.
45. Otwinowski Z, Minor W (1997) Processing of X-ray diffraction data collected in oscillation mode. *Methods Enzymol* 276:307–326.
46. Kabsch W (2010) Integration, scaling, space-group assignment and post-refinement. *Acta Crystallogr D Biol Crystallogr* 66:133–144.
47. Collaborative Computational Project, Number 4 (1994) The CCP4 suite: Programs for protein crystallography. *Acta Crystallogr D Biol Crystallogr* 50:760–763.
48. McCoy AJ, et al. (2007) Phaser crystallographic software. *J Appl Cryst* 40:658–674.
49. Emsley P, Cowtan K (2004) Coot: Model-building tools for molecular graphics. *Acta Crystallogr D Biol Crystallogr* 60:2126–2132.
50. Murshudov GN, Vagin AA, Dodson EJ (1997) Refinement of macromolecular structures by the maximum-likelihood method. *Acta Crystallogr D Biol Crystallogr* 53: 240–255.
51. Modak HV, Kelly DJ (1995) Acetyl-CoA-dependent pyruvate carboxylase from the photosynthetic bacterium *Rhodobacter capsulatus*: Rapid and efficient purification using dye-ligand affinity chromatography. *Microbiology* 141:2619–2628.
52. Terzaghi BE, Sandine WE (1975) Improved medium for lactic streptococci and their bacteriophages. *Appl Microbiol* 29:807–813.
53. Wells JM, Wilson PW, Le Page RW (1993) Improved cloning vectors and transformation procedure for *Lactococcus lactis*. *J Appl Bacteriol* 74:629–636.
54. Maguin E, Prévost H, Ehrlich SD, Gruss A (1996) Efficient insertional mutagenesis in lactococci and other gram-positive bacteria. *J Bacteriol* 178:931–935.
55. Zhang G, Mills DA, Block DE (2009) Development of chemically defined media supporting high-cell-density growth of lactococci, enterococci, and streptococci. *Appl Environ Microbiol* 75:1080–1087.
56. Leloup L, Ehrlich SD, Zagorec M, Morel-Deville F (1997) Single-crossover integration in the *Lactobacillus sake* chromosome and insertional inactivation of the *ptsI* and *lacL* genes. *Appl Environ Microbiol* 63:2117–2123.
57. Lo R, et al. (2009) Cystathionine gamma-lyase is a component of cystine-mediated oxidative defense in *Lactobacillus reuteri* BR11. *J Bacteriol* 191:1827–1837.